PHYSICAL REVIEW D **82,** 043513 (2010)

CMB constraints on principal components of the inflaton potential

Cora Dvorkin[1,2] and Wayne Hu[1,3]

[1]*Kavli Institute for Cosmological Physics, Enrico Fermi Institute, University of Chicago, Chicago, Illinois 60637, USA*
[2]*Department of Physics, University of Chicago, Chicago, Illinois 60637, USA*
[3]*Department of Astronomy & Astrophysics, University of Chicago, Chicago, Illinois 60637, USA*

(Received 2 July 2010; published 11 August 2010)

We place functional constraints on the shape of the inflaton potential from the cosmic microwave background through a variant of the generalized slow-roll approximation that allows large amplitude, rapidly changing deviations from scale-free conditions. Employing a principal component decomposition of the source function $G' \approx 3(V'/V)^2 - 2V''/V$ and keeping only those measured to better than 10% results in 5 nearly independent Gaussian constraints that may be used to test any single-field inflationary model where such deviations are expected. The first component implies $<3\%$ variations at the 100 Mpc scale. One component shows a 95% CL preference for deviations around the 300 Mpc scale at the $\sim 10\%$ level but the global significance is reduced considering the 5 components examined. This deviation also requires a change in the cold dark matter density which in a flat ΛCDM model is disfavored by current supernova and Hubble constant data and can be tested with future polarization or high multipole temperature data. Its impact resembles a local running of the tilt from multipoles 30–800 but is only marginally consistent with a constant running beyond this range. For this analysis, we have implemented a $\sim 40\times$ faster WMAP7 likelihood method which we have made publicly available.

DOI: 10.1103/PhysRevD.82.043513 PACS numbers: 98.80.Cq, 98.70.Vc, 98.80.Es

I. INTRODUCTION

Under the assumption that cosmological perturbations were generated during an inflationary period from quantum fluctuations in a single scalar field, features in the cosmic microwave background (CMB) temperature and polarization power spectra constrain features in the inflaton potential $V(\phi)$.

The usual slow-roll assumption of a small and nearly constant dimensionless slope $(V'/V)^2$ and curvature (V''/V) of the inflaton potential leads to featureless power law initial curvature fluctuations. Breaking any of these assumptions leads to features in the initial spectrum. Indeed glitches in the observed temperature power spectrum of the CMB [1] have led to recent interest in exploring models with strong features in the potential (e.g. [2–9]). The significance at which such models are favored is difficult to address due to the *a posteriori* manner in which they were chosen.

Here we take a more model independent approach to constraining the shape of the inflaton potential. We have recently shown that even in the presence of large local changes in the curvature of the inflaton potential that can explain the glitches, there is to excellent approximation only a single function of the inflaton potential that the observations constrain [8]. Moreover, this function is approximately the same combination of slope and curvature that enters into the calculation of the scalar tilt in the ordinary slow-roll approximation. In this generalized slow-roll (GSR) formalism this quantity need not be small or constant [10–12]. With it, one can bypass a parametrization of the initial curvature power spectrum (e.g. [13–19]) and the problem that not all spectra correspond to possible inflationary models.

In this paper, we take a principal components approach [20] to functional constraints on the inflaton potential under the GSR formalism. Principal components constructed *a priori* from a noise model of the WMAP CMB measurements determine the theoretically best constrained deviations from a featureless potential before examining the actual data. Constraints from the low-order principal components thus efficiently encapsulate the expected information content of the data and may be used to test a variety of inflationary models without a reanalysis of the data.

We begin in Sec. II with a brief review of the GSR formalism. In Sec. III B we develop the principal component analysis of the GSR source function and apply it to the WMAP 7 yr (WMAP7) data in Sec. IV. In Sec. V we consider applications of these derived constraints on the inflaton potential and discuss these results in Sec. VI. In the Appendix, we present the fast likelihood approach to the WMAP7 data employed in these analyses.

II. GENERALIZED SLOW ROLL

Given a specific model for the inflaton potential, the initial curvature fluctuation spectrum can always be numerically computed by solving the linearized scalar field equation. The slow-roll approaches, however, provide

model independent mappings from the inflaton potential to the curvature spectrum provided that the requisite approximations hold.

The generalized slow-roll (GSR) formalism was originally developed to consider cases where the usual slow-roll parameters $\epsilon_H \equiv (\dot{\phi}/H)^2/2$ and $\eta_H \equiv -\ddot{\phi}/H\dot{\phi}$ are small but η_H is not necessarily constant [10–12]. Here ϕ is the inflaton field and overdots represent derivatives with respect to coordinate time t. In a previous paper [8], we have shown that a variant of GSR works well for cases where η_H becomes of order unity for a fraction of an e-fold.

In this variant of the GSR approximation, the curvature power spectrum is a nonlinear functional

$$\ln\Delta^2_{\mathcal{R}}(k) \approx G(\ln\eta_{\rm min}) + \int_{\eta_{\rm min}}^{\eta_{\rm max}} \frac{d\eta}{\eta} W(k\eta) G'(\ln\eta) + \ln\left[1 + \frac{1}{2}\left(\int_{\eta_{\rm min}}^{\eta_{\rm max}} \frac{d\eta}{\eta} X(k\eta) G'(\ln\eta)\right)^2\right], \quad (1)$$

of the function

$$G'(\ln\eta) = \frac{2}{3}\left(\frac{f''}{f} - 3\frac{f'}{f} - \frac{f'^2}{f^2}\right) \quad (2)$$

which is related to the inflaton potential through the background solution $f = 2\pi\dot{\phi}a\eta/H$. Primes here and below denote derivatives with respect to $\ln\eta$ and $\eta = \int_t^{t_{\rm end}} dt'/a$ is the conformal time to the end of inflation. We require $k_{\rm max}\eta_{\rm min} \ll 1$ and $k_{\rm min}\eta_{\rm max} \gg 1$ for the range in k that we are calculating the spectrum. Integrating G' gives

$$G(\ln\eta) = \ln\left(\frac{1}{f^2}\right) + \frac{2}{3}\frac{f'}{f}. \quad (3)$$

The window functions

$$W(u) = \frac{3\sin(2u)}{2u^3} - \frac{3\cos 2u}{u^2} - \frac{3\sin(2u)}{2u},$$
$$X(u) = -\frac{3\cos(2u)}{2u^3} - \frac{3\sin(2u)}{u^2} + \frac{3\cos(2u)}{2u} + \frac{3}{2u^3}(1+u^2), \quad (4)$$

define the linear and nonlinear response of the curvature spectrum to G' respectively. For the models we consider, the nonlinear response is small compared with the linear one.

The key property of Eq. (1) is that deviations from scale invariance in the curvature spectrum depend only on a single function of time G'. Moreover, to good approximation, this function is related to the inflaton potential as [8]

$$G' \approx 3\left(\frac{V_{,\phi}}{V}\right)^2 - 2\frac{V_{,\phi\phi}}{V}, \quad (5)$$

so long as $|\eta_H'| \gg |\eta_H|$ when η_H is large, i.e. that η_H remains large only for a fraction of an e-fold [8]. Finally, if the ordinary slow-roll approximation where ϵ_H and η_H are both small and nearly constant holds, then G' may be evaluated at horizon crossing $\eta \approx k^{-1}$ and taken out of the integrals in Eq. (1). As we shall see below, under this approximation $G' = 1 - n_s$. By allowing G' to be both time varying and potentially large, we recover ordinary slow-roll results where they apply but allow the data themselves to test their validity.

III. PRINCIPAL COMPONENTS

The GSR approximation allows us to go beyond specific models of inflation in examining how the data constrain the inflaton potential. The data directly constrain the function G' and hence the derivatives of the inflaton potential through Eq. (5).

Given that G' is related to the curvature spectrum $\Delta^2_{\mathcal{R}}$ by an integral relation and the curvature spectrum itself is related to the observable CMB power spectra by a line-of-sight integration, not all aspects of the function G' are observable even with perfect data.

We therefore seek a basis for an efficient representation of *observable* properties of G'. We begin in Sec. III A with a general description of a basis expansion for G' and its relationship to the usual normalization and tilt parameters. We then turn in Sec. III B to principal components (PCs) as the basis which best encapsulates expected deviations from scale-free conditions [20].

A. Basis expansion

In general, we seek to represent the function G' as

$$G'(\ln\eta) = \sum_{a=0}^{N} m_a S_a(\ln\eta), \quad (6)$$

where the basis functions S_a for $a > 0$ are assumed to have compact support in some region between $\ln\eta_{\rm min}$ and $\ln\eta_{\rm max}$ corresponding to the range probed by the data. We assume $S_0 = 1$ so that within this range m_0 represents a constant tilt in the spectrum.

We seek functions that obey the orthogonality and completeness relations

$$\frac{1}{\Delta\ln\eta}\sum_a S_a(\ln\eta)S_a(\ln\eta') = \delta(\ln\eta - \ln\eta'),$$
$$\frac{1}{\Delta\ln\eta}\int d\ln\eta S_a(\ln\eta)S_b(\ln\eta) = \delta_{ab}, \quad (7)$$

where $\Delta\ln\eta = \ln\eta_{\rm max} - \ln\eta_{\rm min}$. From these relations, the m_a amplitudes are related to G' as

$$m_a = \frac{1}{\Delta\ln\eta}\int d\ln\eta S_a(\ln\eta) G'(\ln\eta). \quad (8)$$

Note that our normalization differs from that of Ref. [20] in that unit amplitude m_a corresponds to unit variance in G' averaged over the whole range in $\ln\eta$.

Substituting this model into the power spectrum expression (1) yields

$$\ln\Delta^2_{\mathcal{R}}(k) \approx G(\ln\eta_{\rm min}) + m_0 C - m_0 \ln(k\eta_{\rm min}) + \sum_{a=1}^{N} m_a W_a(k) + \ln\left[1 + \frac{1}{2}\left(\sum_{a=0}^{N} m_a X_a(k)\right)^2\right], \quad (9)$$

where $C = \frac{7}{3} - \gamma_{\rm E} - \ln 2 \approx 1.06297$ with $\gamma_{\rm E}$ as the Euler-Mascheroni constant, $X_0 = \pi/2$. The k-space responses to the modes are characterized by

$$W_a(k) = \int_{\eta_{\rm min}}^{\eta_{\rm max}} d\ln\eta W(k\eta) S_a(\ln\eta),$$
$$X_a(k) = \int_{\eta_{\rm min}}^{\eta_{\rm max}} d\ln\eta X(k\eta) S_a(\ln\eta),$$

where $k\eta_{\rm min} \ll 1$ and $k\eta_{\rm max} \gg 1$. Note that if $m_a = 0$ for $a > 0$

$$\Delta^2_{\mathcal{R}}(k) = e^{G(\ln\eta_{\rm min}) + m_0 C}\left(1 + \frac{\pi^2}{8} m_0^2\right)(k\eta_{\rm min})^{-m_0} \quad (10)$$

from which we infer that the model is a pure power law spectrum. We can therefore choose instead to represent $G(\ln\eta_{\rm min})$ and m_0 by n_s and A_s bringing our parameterization of the power spectrum to

$$\ln\Delta^2_{\mathcal{R}} = \ln\left[A_s\left(\frac{k}{k_p}\right)^{n_s - 1}\right] + \sum_{a=1}^{N} m_a W_a(k) + \ln\left[1 + \frac{1}{2}\left(\frac{\pi}{2}(1 - n_s) + \sum_{a=1}^{N} m_a X_a(k)\right)^2\right]. \quad (11)$$

Note that this replacement ensures that the normalization and tilt parameters are defined at a scale k_p that is well-constrained by the data. Hence any small and unobservable running of G and G' from $\eta_{\rm min}$ to $\eta \sim 1/k_p$ is absorbed into A_s and n_s respectively. Nonzero values of $m_{a>0}$ required by the data thus represent a deviation from purely scale-free initial conditions.

We hereafter consider Eq. (11) as the definition of the parametrized curvature power spectrum. In practice we choose $k_p = 0.05$ Mpc^{-1}, and for reference note that $k \approx 0.02$ Mpc^{-1} for modes contributing to the well-measured first acoustic peak.

B. Principal component basis

We choose here to construct the basis functions S_a from the principal components (PCs) of the projected WMAP7 covariance matrix for perturbations in G'. To define the PCs, we begin with a fiducial flat ΛCDM model with a scale-free initial spectrum. We take the baryon density to be $\Omega_b h^2 = 0.02268$, cold dark matter density $\Omega_c h^2 = 0.1080$, cosmological constant $\Omega_\Lambda = 0.7507$, optical depth $\tau = 0.089$, $A_s = 2.41 \times 10^{-9}$, $n_s = 0.96$ and $m_{a>0} = 0$. This model corresponds to a constant $G' = 0.04$.

We then construct the PCs as the theoretically best constrained nonconstant deviations in G' around this fiducial model. We start by adding a set of perturbations in $G'(\ln\eta_i) = 0.04 + p_i$ at 50 equally spaced intervals in $\ln\eta$ between $1 < \eta/{\rm Mpc} < 10^5$. From this set, we define the function $G'(\ln\eta)$ by a cubic spline. This sampling of 10 per decade or $\delta\ln\eta = 0.23$ across $\Delta\ln\eta = 11.5$ is sufficient to capture the observable properties of G' barring unphysical models with both high frequency and high amplitude perturbations. The spline ensures a smooth interpolation between the samples.

To these parameters p_i we add the cosmological parameters

$$p_\mu = \{p_i, A_s, n_s, \tau, \Omega_b h^2, \Omega_c h^2, \theta\}, \quad (12)$$

where the angular extent of the sound horizon θ takes the place of Ω_Λ, and construct the Fisher matrix

$$F_{\mu\nu} = \sum_{\ell=2}^{\ell_{\rm max}} \sum_{XY,\tilde{X}\tilde{Y}} \frac{\partial C_\ell^{XY}}{\partial p_\mu} \mathbf{C}^{-1}_{XY\tilde{X}\tilde{Y}} \frac{\partial C_\ell^{\tilde{X}\tilde{Y}}}{\partial p_\nu}, \quad (13)$$

where the XY pairs run over the observable power spectra TT, EE, TE. For the data covariance matrix, we take

$$\mathbf{C}_{XY\tilde{X}\tilde{Y}} = \frac{1}{(2\ell+1) f_{\rm sky}}[(C_\ell^{X\tilde{X}} + N_\ell^{X\tilde{X}})(C_\ell^{Y\tilde{Y}} + N_\ell^{Y\tilde{Y}}) + (C_\ell^{X\tilde{Y}} + N_\ell^{X\tilde{Y}})(C_\ell^{Y\tilde{X}} + N_\ell^{Y\tilde{X}})], \quad (14)$$

where the WMAP7 noise power $N_\ell^{X\tilde{X}} = \delta_{X\tilde{X}} N_\ell^{XX}$ is inferred from the temperature power spectrum errors from the LAMBDA site [21] and the assumption that $N_\ell^{EE} = 2N_\ell^{TT}$. We set $\ell_{\rm max} = 1200$ and $f_{\rm sky} = 1$.

We then invert the Fisher matrix to form the covariance matrix $\mathbf{C} = \mathbf{F}^{-1}$. Next we take the sub-block C_{ij} and decompose it with the orthonormal matrix S_{ja},

$$C_{ij} = \frac{\Delta\ln\eta}{\delta\ln\eta} \sum_a S_{ia} \sigma_a^2 S_{ja} \quad (15)$$

rank ordered from lowest to highest σ_a. Each eigenvector defines a discrete sampling of the basis function S_a via

$$S_a(\ln\eta_i) = \sqrt{\frac{\Delta\ln\eta}{\delta\ln\eta}} S_{ia}, \quad (16)$$

with the normalization of Eq. (7). The full functions $S_a(\ln\eta)$ are defined by taking a cubic spline through the samples. The first 5 PC components are shown in Fig. 1.

In the Fisher approximation σ_a represents the WMAP7 expected errors for m_a

$$\langle m_a m_b \rangle = \delta_{ab} \sigma_a^2, \quad (17)$$

for a zero mean fiducial model $\langle m_a \rangle = 0$.

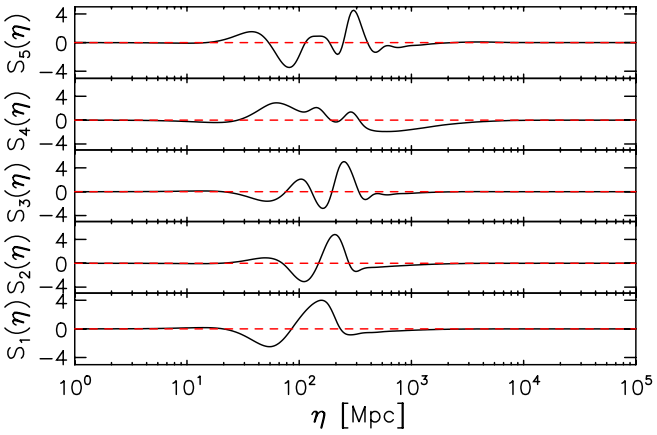

FIG. 1 (color online). The first 5 principal components (PCs) of G' as a function of conformal time based on the WMAP7 specifications. The power law model with zero amplitude PCs is shown in red dashed lines. The first 5 PCs represent a local expansion of G' around $\eta \sim 10^2$ Mpc.

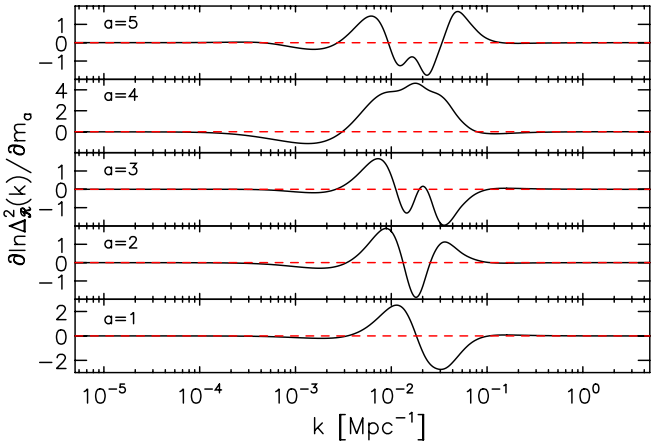

FIG. 3 (color online). Sensitivity of the curvature power spectrum to the first 5 PC parameters. Low-order PCs mainly change the power spectrum at wave number in the decade around $k \sim 10^{-2}$ Mpc^{-1}. The red dashed line represents the zero PC amplitude fiducial power law model.

These errors are shown in Fig. 2. Note that the noise rises by a factor of 4 across the first 5 components and then increases to order unity by the 20th component. Given that the peak amplitudes of S_a lie in the $\sim$4 range, a $\sim$2.5% error corresponds to a $\sim$10% peak variation in G' or the effective tilt. By keeping the first 5 PCs, we retain all of the constraints on deviations in G' in the 10% range. In this sense, these 5 modes represent the best set for examining deviations from a scale-free power law model. Note that no actual WMAP7 data goes into the construction and so that the modes are chosen *a priori* rather than *a posteriori*.

For the first 5 PC components, the S_a basis functions are centered near $\eta \approx 10^2$ Mpc and reflect the strong WMAP sensitivity to the first peak at $\ell \approx 200$ or $k \sim 0.02$ Mpc^{-1} in the fiducial model. The first 5 components resemble a local decomposition of G' in the decade surrounding this scale. This fact can be seen more directly by examining the sensitivity of the curvature and temperature power spectra to the 5 PC amplitudes (see Figs. 3 and 4, respectively).

As an example of the utility of retaining only the first 5 PCs, consider a linear model for G'

$$G'(\ln\eta) = 1 - n_s + \alpha \ln(\eta/\eta_0). \tag{18}$$

The local slope in the power spectrum in the GSR approximation is

$$\frac{d\ln\Delta^2_{\mathcal{R}}}{d\ln k} = n_s - 1 + \alpha \ln(k\eta_0), \tag{19}$$

and so $\alpha = dn_s/d\ln k$ and is equivalent to the running of the tilt. This linear model can be projected onto the first 5

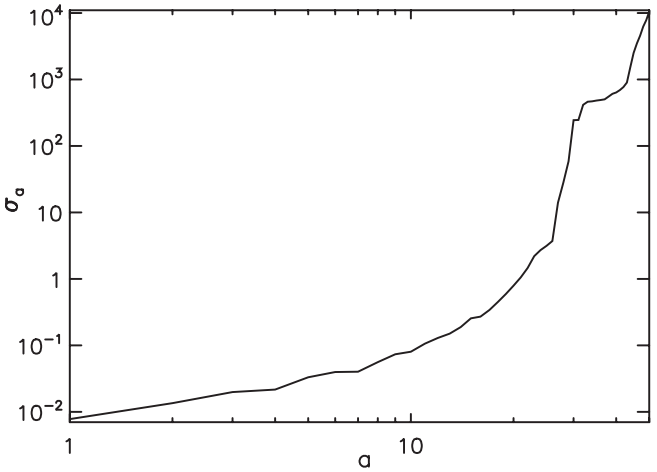

FIG. 2. Predicted RMS error on the PC amplitudes as a function of mode number for WMAP7 data. PCs are rank ordered from lowest to highest error with the first 5 describing modes with better than $\sim$10% constraints on G'.

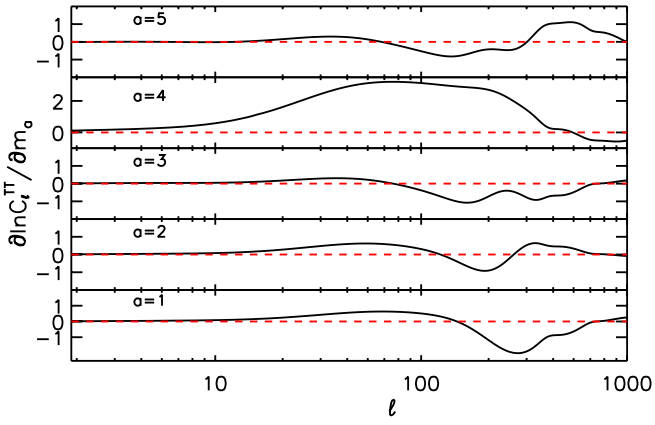

FIG. 4 (color online). Sensitivity of the temperature power spectrum to the first 5 PC parameters. Low-order PCs represent slowly varying features around the first peak $\ell \sim 200$. The red dashed line represents the zero PC amplitude fiducial power law model.

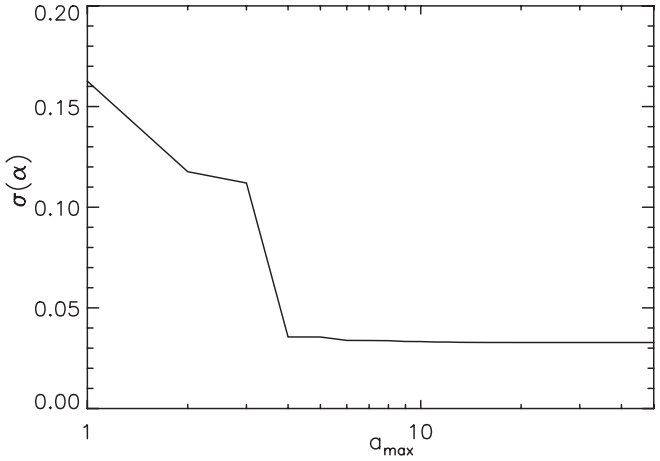

FIG. 5. Predicted RMS errors on running of tilt α as a function of the maximum number of PC components included. Note that the errors cease to improve after the first 4 components and most of the improvement comes from the 4th component.

PCs. The variance of α is then given by

$$\frac{1}{\sigma^2(\alpha)} = \sum_{a=1}^{a_{\max}} \frac{1}{\sigma_a^2}\left(\frac{\partial m_a}{\partial \alpha}\right)^2, \tag{20}$$

where

$$\frac{\partial m_a}{\partial \alpha} = \frac{1}{\Delta \ln \eta} \int d\ln\eta S_a(\ln\eta) \ln(\eta/\eta_0). \tag{21}$$

By virtue of the marginalization of n_s in the construction of the PCs, the S_a functions have nearly zero mean and $\partial m_a/\partial\alpha$ does not depend on the scale η_0 where the effective tilt is defined as $G'(\ln\eta_0) = 1 - n_s$.

Figure 5 shows the predicted RMS error on α as a function of the maximum PC mode retained. With 5 PCs, $\sigma(\alpha) = 0.0355$, while the fully-saturated value of the error with 50 PCs is $\sigma(\alpha) = 0.0327$. This should be compared with the projected error using α itself as a Fisher matrix parameter, $\sigma(\alpha) = 0.0328$. These results verify the completeness of the 50 PC basis as well as show that most of the information for $|\alpha| \ll 1$ is expected to come from the first 5 PCs.

In fact most of the information comes from a single mode, the 4th. This mode corresponds to a local variation in the effective tilt G' with a null near 300 Mpc (see Fig. 1), or in the power spectrum near $\sim$0.003 Mpc^{-1} (see Fig. 3), and an extent spanning 1–2 decades. Even though the 1st mode has smaller overall errors and better constrains peak variations in G', it is not the most effective mode for constraining running of the tilt given its extremely local form.

This caveat applies more generally. A given model may have large deviations in G' in a region where the data does not best constrain G'. In this case the first 5 PCs no longer represent a complete or efficient representation. We return to this point in Sec. V.

C. MCMC

We use a Markov Chain Monte Carlo (MCMC) likelihood analysis to determine joint constraints on the first 5 PC amplitudes and cosmological parameters

$$p_\mu = \{m_1, \ldots, m_5, A_s, n_s, \tau, \Omega_b h^2, \Omega_c h^2, \theta\}. \tag{22}$$

On top of this basic set we also examine the impact of spatial curvature Ω_K and tensor-scalar ratio r and the amplitude of a Sunyaev-Zel'dovich contaminant $A_{\rm SZ}$ on a case-by-case basis.

The MCMC algorithm samples the parameter space evaluating the likelihood $\mathcal{L}(\mathbf{x}|\mathbf{p})$ of the data $\mathbf{x}$ given each proposed parameter set $\mathbf{p}$ (e.g. see [22,23]). The posterior distribution is obtained using Bayes' theorem,

$$\mathcal{P}(\mathbf{p}|\mathbf{x}) = \frac{\mathcal{L}(\mathbf{x}|\mathbf{p})\mathcal{P}(\mathbf{p})}{\int d\boldsymbol{\theta}\, \mathcal{L}(\mathbf{x}|\mathbf{p})\mathcal{P}(\mathbf{p})}, \tag{23}$$

where $\mathcal{P}(\mathbf{p})$ is the prior probability density. We place noninformative top-hat priors on all parameters in Eq. (22). For example, for the PC amplitudes we take $\mathcal{P}(m_{a>0}) = 1$ for $-1 \le m_{a>0} \le 1$ and 0 otherwise.

The MCMC algorithm generates random draws from the posterior distribution that are fair samples of the likelihood surface. We test convergence of the samples to a stationary distribution that approximates the joint posterior density $\mathcal{P}(\mathbf{p}|\mathbf{x})$ by applying a conservative Gelman-Rubin criterion [24] of $R - 1 < 0.01$ across four chains. We use the code CosmoMC [25] for the MCMC analysis [26].

For the WMAP7 data [27], we optimize the likelihood code available at the LAMBDA web site as detailed in the Appendix. The net improvement in speed on an 8-core desktop processor is a factor of $\sim$40 which should enable future studies with 20 or more PCs or other initial power spectrum parameters.

IV. CONSTRAINTS

In this section we present the constraints on the 5 best measured principal components of the GSR source function G' and implicitly the inflaton potential $V(\phi)$. We first examine constraints using the WMAP7 data only and then joint with a variety of cosmological constraints to remove residual parameter degeneracies.

A. WMAP

We begin by considering the WMAP7 data in a flat ΛCDM cosmological context. We show the probability distributions of the first 5 PCs and cosmological parameters in Fig. 6. Table I shows the mean, standard deviation of the posterior probabilities as well as the maximum like-

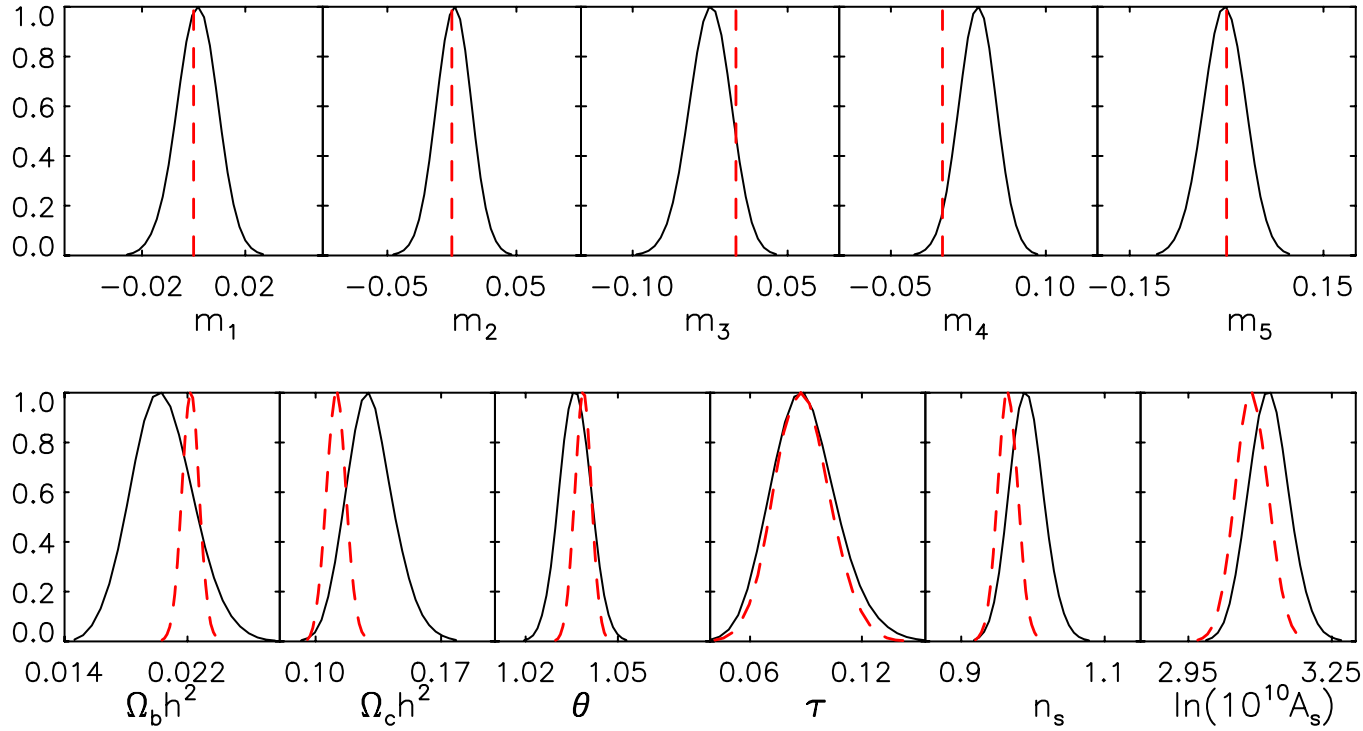

FIG. 6 (color online). Posterior probability distributions of the cosmological and 5 PC parameters using WMAP7 data. The red dashed line represents the power law results where the first 5 PC parameters are held fixed to $m_a = 0$.

lihood parameter values for the power law models vs the 5PC models.

For visualization purposes we show in Fig. 7 the functional posterior probability of

$$G_5'(\eta) \equiv 1 - n_s + \sum_{a=1}^{5} m_a S_a(\eta), \tag{24}$$

which should be interpreted as G' filtered through the first 5 PCs and *not* a reconstruction of G' itself.

All 5 PCs are tightly constrained, with errors that are comparable to the Fisher matrix projection, nearly Gaussian posteriors and little covariance with each other. The correlation coefficients between two different m_a's, $|C_{m_a m_b}/\sigma(m_a)\sigma(m_b)| < 0.2$. The first component m_1 in

TABLE I. Means, standard deviations (left subdivision of columns) and maximum likelihood values (right subdivision of columns) with likelihood values for ΛCDM and the 5 PCs model with WMAP7 data.

Parameters	Power Law (PL)		Principal Components (PC)	
$100\Omega_b h^2$	2.220 ± 0.055	2.217	2.040 ± 0.196	2.067
$\Omega_c h^2$	0.1116 ± 0.0053	0.1130	0.1308 ± 0.0127	0.1284
θ	1.0386 ± 0.0026	1.0387	1.0361 ± 0.0049	1.0365
τ	0.088 ± 0.014	0.088	0.089 ± 0.017	0.088
n_s	0.9650 ± 0.0136	0.9622	0.9916 ± 0.0233	0.9877
$\ln[10^{10}A_s]$	3.083 ± 0.034	3.088	3.119 ± 0.041	3.105
m_1	0	0	0.0014 ± 0.0077	0.0021
m_2	0	0	0.0015 ± 0.0132	0.0068
m_3	0	0	-0.0253 ± 0.0197	−0.0264
m_4	0	0	0.0339 ± 0.0175	0.0337
m_5	0	0	-0.0033 ± 0.0315	0.0023
H_0	70.13 ± 2.38	69.50	61.41 ± 6.08	62.18
Ω_Λ	0.726 ± 0.028	0.720	0.581 ± 0.116	0.614
$-2\ln\mathcal{L}$	7474.97		7469.82	

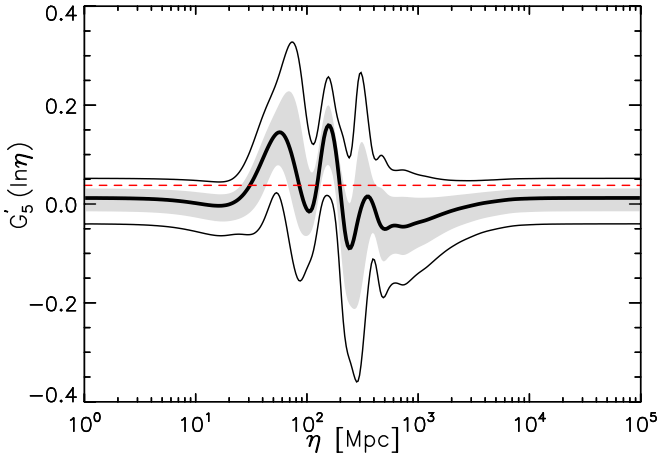

FIG. 7 (color online). The 5 PC filtered G_5' posterior using WMAP7 data. The shaded region encloses the 68% CL region and the upper and lower curves show the upper and lower 95% CL limits. The maximum likelihood (ML) G_5' is shown as the thick central curve, and the power law ML model is shown in red dashed lines. Structure in this representation mainly reflects the form of the PC modes and is dominated by the modes with the largest uncertainties.

particular is consistent with zero and places the tightest constraints of $\lesssim 3\%$ local variations in G' around $\eta \approx 10^2$ Mpc. Interestingly, the power law prediction of $m_4 = 0$ lies in the tails of the posterior with as extreme or more values disfavored at 94.8% CL. With the Gaussian approximation $m_4 = 0$ is 1.9σ from the mean and disfavored at 94.5% CL.

In Fig. 8, we show joint posteriors of the PCs with other parameters. Notably, for the anomalous m_4 component there is a degeneracy with $\Omega_c h^2$, $\Omega_b h^2$ and n_s which is also reflected in the broadening of the cosmological parameter posteriors in Fig. 6 and the shift in means and maximum likelihood values in Table I. The maximum likelihood (ML) model found by the chain is an improvement over the power law case of $2\Delta \ln\mathcal{L} \approx 5$ which is marginal considering the addition of 5 parameters.

The intriguing aspect of the ML model, like the m_a posteriors, is that the improvement is concentrated in the m_4 component. Note that the finite m_4 component allows $n_s = 1$ to be a good fit to the data implying that the data can be marginally better fit by a local deviation from scale invariance rather than tilt.

An examination of the ML model helps illuminate the degeneracies with cosmological parameters. Figure 9 (top) shows the temperature power spectra of the 5 PC ML model compared to the power law ML model (upper panel), and the fractional difference between the two (lower panel). Note that in the well-constrained $\ell \sim$ 30–800 regime the two spectra agree to $\sim$1% or better. This accidental degeneracy is not preserved beyond $\ell = 1000$. Furthermore the E-mode polarization power spectra shown in Fig. 9 (bottom) reveal substantially larger fractional deviations of up to $\sim$10% that break the degeneracy in the temperature spectra.

Indeed the main improvement of the PC model relative to the PL model actually comes from the $\ell \geq 24$ polarization cross correlation part of the likelihood (MASTER *TETE*), where $2\Delta \ln\mathcal{L} = 3.5$, with half of this contribution coming from $\ell < 200$. The low-ℓ temperature part of the likelihood has an improvement of $2\Delta \ln\mathcal{L} = 1.8$ relative to the PL model, and there is a smaller improvement coming from the high-ℓ (MASTER *TT*) part with $2\Delta \ln\mathcal{L} = 1.1$. Finally, the PC model is worse than the PL model by $2\Delta \ln\mathcal{L} = -1.3$ for the low $\ell < 24$ polarization.

The intermediate ℓ temperature degeneracy exhibited by the two models is further explored in Fig. 10. We show the impact of the cumulative parameter variations between the PL and PC ML models. The addition of m_4 carries almost all of the impact of the PCs and is mainly compensated by variations in $\Omega_c h^2$ to adjust the relative heights of the peaks and n_s to tilt the spectrum to small scales. The change in $\Omega_c h^2$ also changes the physical size of the sound horizon which must be compensated by a change in the distance to recombination reflected in a lower value for H_0 and Ω_Λ to leave the angular scale θ compatible with the data.

These results are robust to marginalizing Ω_K given any reasonable prior on H_0, an SZ component through $A_{\rm SZ}$, or tensors within the B-mode measured limits of the BICEP experiment $r = 0.03^{+0.31}_{-0.26}$ [28]. Through an explicit MCMC analysis of these separate cases, we have verified that the shift in the means and change in the errors for all 5 PCs are much smaller than 1σ. The largest effect is from marginalizing tensors where for example $m_4 = 0.042 \pm 0.20$. A small improvement in the B-mode limits would eliminate this ambiguity entirely.

B. Joint constraints

The results of the previous section suggest that other data which measure the high-ℓ temperature spectrum, polarization spectrum, or pin down the cosmological parameters that control the distance to recombination and baryon density can eliminate the remaining degeneracies and enable WMAP7 to better constrain the inflaton potential.

We start with adding more CMB information from the QUAD experiment. QUAD helps mainly by reducing the $m_5 - \Omega_b h^2$ degeneracy. Interestingly, most of the impact comes from the polarization measurements rather than the extended range of the temperature constraints.

Adding in non-CMB cosmological information helps even more, especially with m_4. We take the UNION2 supernovae data set [29], the SHOES $H_0 = (74.2 \pm 3.6)$ km/s/Mpc measurement [30] and a big bang nucleosynthesis constraint of $\Omega_b h^2 = 0.022 \pm 0.002$. In a flat ΛCDM cosmology, the degeneracy between m_4 and

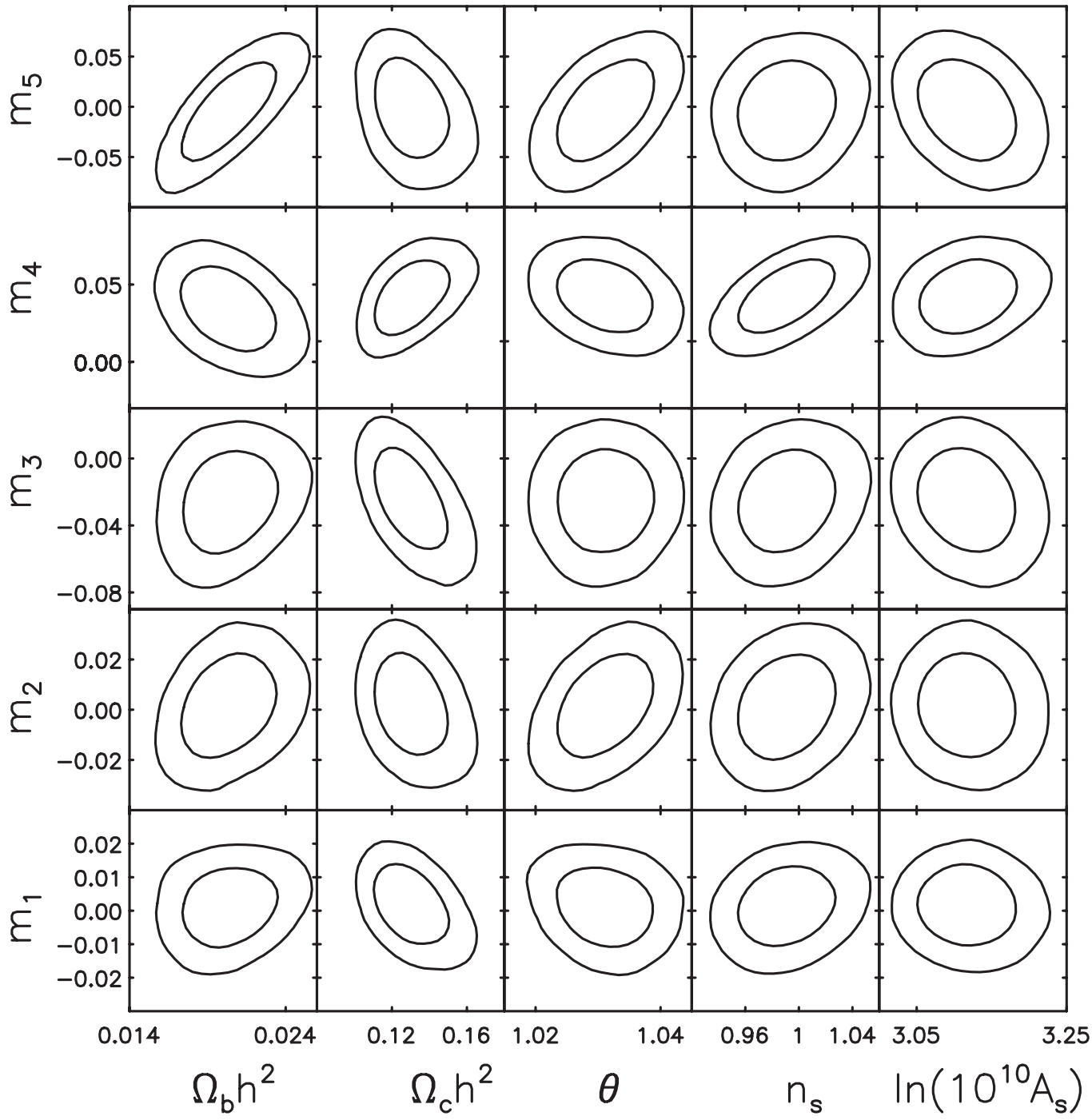

FIG. 8. Joint probability distributions of the principal component amplitudes and the cosmological parameters from MCMC analysis of WMAP7 data (68% and 95% CL contours).

$\Omega_c h^2$ is nearly eliminated yielding $m_4 = 0.0191 \pm 0.0163$, i.e. consistent with power law initial conditions. Of the additional data it is the supernovae that drive this improvement by disfavoring the low Ω_Λ values required by the increase in $\Omega_c h^2$.

On the other hand, these improvements require an assumption that the dark energy is a cosmological constant and the Universe is spatially flat. For example if Ω_K is marginalized, $m_4 = 0.0384 \pm 0.0197$. The addition of spatial curvature allows the freedom to adjust the relative distance to the high-z supernova and recombination. A better measurement of H_0 could resolve this degeneracy since the constraints on Ω_K are already limited by the SHOES data.

Table II summarizes these results for the constraints on the PC amplitudes.

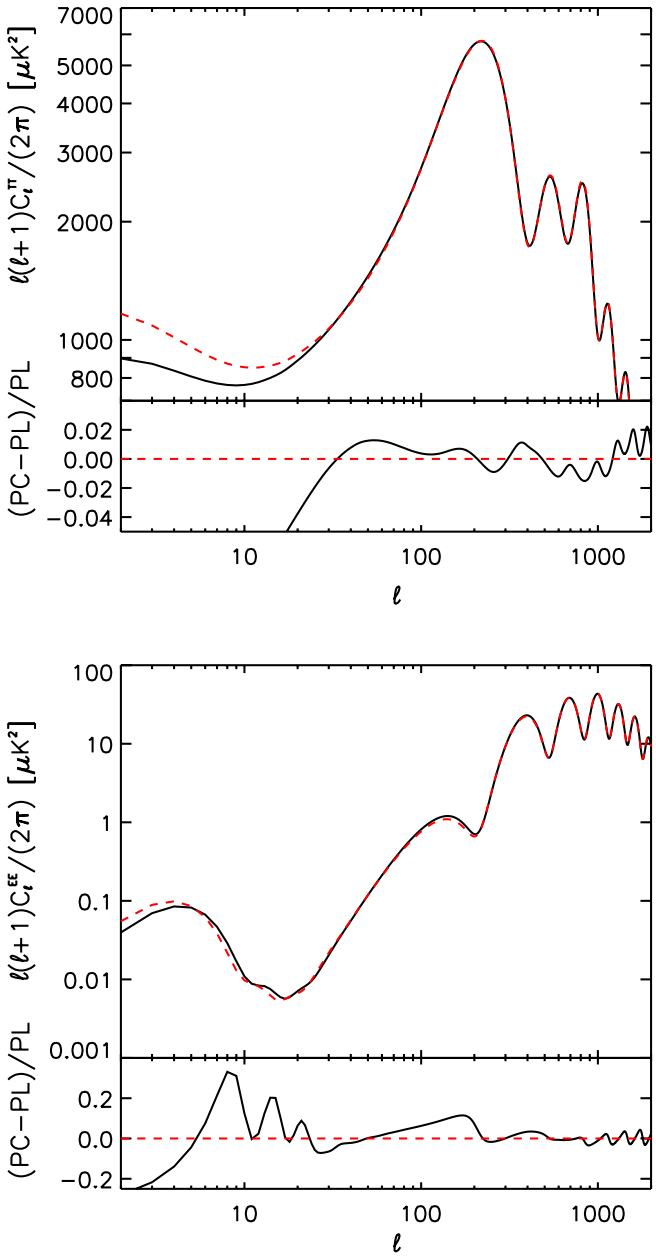

FIG. 9 (color online). Power spectra of the 5 PCs maximum likelihood model (black curve) compared to power law (PL) maximum likelihood model (red dashed curve) in the upper panel, and the difference (PC − PL)/PL in the lower panel. Top: temperature power spectrum. Bottom: polarization power spectrum.

V. APPLICATIONS

The model independent results of the previous section can be used to test a wide variety of inflationary deviations from scale-free conditions. Moreover given that the constraints on the PC amplitudes are uncorrelated and approximately Gaussian, these tests are straightforward to apply.

As the simplest example, take the running of the tilt model defined by $\alpha = dn_s/d\ln k$ through Eq. (18). Using

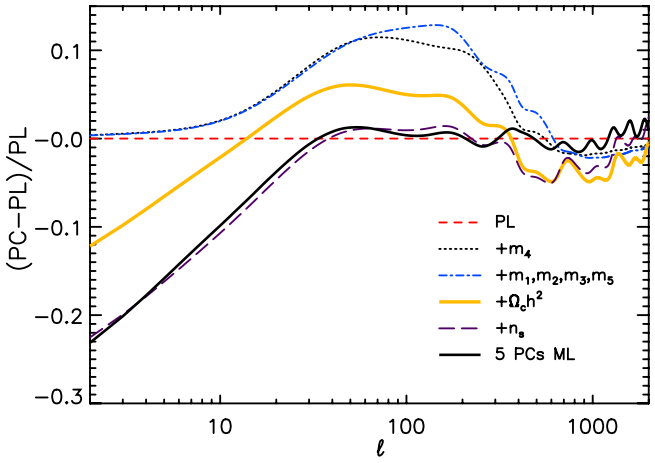

FIG. 10 (color online). Decomposition of the fractional difference between the PC and power law (PL) maximum likelihood models (ML) shown in Fig. 9 into contributions from specific parameters. Curves show the cumulative effect of adjusting the PL ML parameters to the PC ML values. The main effects come from the change in m_4, $\Omega_c h^2$, and n_s.

Eq. (8), we obtain

$$m_1 = 0.048\alpha, \quad m_2 = -0.079\alpha, \quad m_3 = 0.054\alpha, \quad m_4 = -0.576\alpha, \quad m_5 = -0.034\alpha. \tag{25}$$

We can then construct the effective χ^2 statistic

$$\chi^2(\alpha) = \sum_{a=1}^{5}\left[\frac{m_a(\alpha) - \bar{m}_a}{\sigma_a}\right]^2. \tag{26}$$

With the means and variances taken from Table I for WMAP7 we obtain $\alpha = -0.057 \pm 0.029$. When we take into account the covariance between the PC amplitudes, we obtain a 3% shift in the mean with the same error: $\alpha = -0.059 \pm 0.029$. Likewise we have verified that using Eq. (25) in a separate MCMC analysis gives consistent results $\alpha = -0.058 \pm 0.030$.

This result should be compared with the direct analysis of the running of the tilt which gives $\alpha = -0.034 \pm 0.027$ consistent with the analysis from [27]. The mean is shifted from the PC derived mean by $\sim 0.8\sigma$ while the errors are 7% higher.

The small shift in the mean is driven mainly by the truncation to 5 PC components. This is in spite of the Fisher expectation in Sec. III that for an infinitesimal α the first 5 PC components contain nearly all the information. A running of the tilt model where $\alpha = -0.057$, which fits the intermediate $\ell \sim 30$–800 range well, implies a large change across the extended observable range from $\eta \sim 20$–5000 Mpc of $|\delta G'| \sim |\delta n_s| \sim 0.3$. In particular, it overpredicts the suppression of the $\ell < 30$ temperature multipoles. For the same amplitude and tilt at the first peak, the amplitude at the horizon is suppressed by $\sim e^{(\alpha/2)\ln^2(100)} = 0.55$. This suppression can only be par-

TABLE II. Means and standard deviations of the posterior probabilities of the PC amplitudes with different data sets added to the WMAP7 data. For supernovae (SN) we used the UNION2 data set, and for H_0 the SHOES measurement.

PC	+QUAD	+BBN + SN + H_0, flat	+BBN + SN + H_0, w/Ω_K
m_1	0.0000 ± 0.0072	0.0045 ± 0.0071	0.0027 ± 0.0073
m_2	0.0033 ± 0.0123	0.0091 ± 0.0121	0.0045 ± 0.0125
m_3	-0.0261 ± 0.0184	-0.0120 ± 0.0166	-0.0208 ± 0.0178
m_4	0.0296 ± 0.0168	0.0191 ± 0.0163	0.0384 ± 0.0197
m_5	0.0149 ± 0.0250	0.0187 ± 0.0249	0.0091 ± 0.0256

tially compensated by red tilting the spectrum without oversuppressing the high $\ell > 800$ multipoles. Note that cosmic variance completely dominates the uncertainties in the $\ell < 30$ region and decreases with the predicted signal, an effect that is not represented in the Fisher matrix.

In other words, the 2σ preference for finite m_4 is not completely consistent with a constant running of the tilt but rather points to a more local deviation from scale-free conditions. When we eliminate this preference by adding in the additional SN, H_0 and BBN constraints the inferred limits on α from the first 5 PC amplitudes become $\alpha = -0.033 \pm 0.027$. Note however that the direct constraints on α also improve with the addition of these data sets to $\alpha = -0.013 \pm 0.021$.

In Fig. 11 we plot an $\alpha = -0.033$ model for the 5 PCs filtered G'_5 against the posterior constraints from the WMAP7 data and additional SN, H_0 and BBN constraints in a flat universe. We overplot the original unfiltered G' for this α and note that even with the reduced value the deviations become large outside of the region probed by the first 5 PCs.

This example points out a caveat to the use of the first 5 PCs as general constraints on models. For a model with features that are substantially larger in a regime away from the well-constrained first acoustic peak, the first 5 PCs may not be the best constraints in terms of signal-to-noise. One can check whether this is the case by examining the predicted G' or by projecting the model onto the full 50 PC space and checking for large amplitude components. Indeed if the higher components are extremely large compared with the low components, nonlinear effects can break the orthogonality of PCs and lead to larger allowed variations in the low components when compensated by the high components.

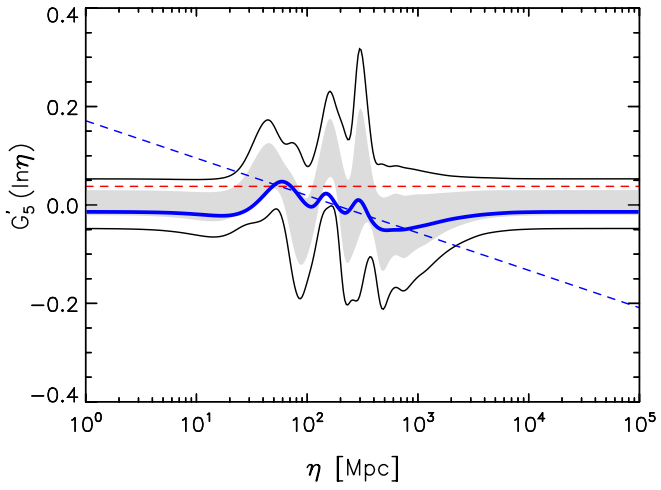

FIG. 11 (color online). The 5 PC filtered G'_5 posterior using WMAP7 data and additional SN, H_0 and BBN constraints in a flat universe. The shaded region encloses the 68% CL region and the upper and lower curves show the upper and lower 95% CL limits. A model with running of the tilt $\alpha = -0.033$, the mean value given these constraints, is shown as the thick solid blue curve and the ML PL model as the dashed red curve. The unfiltered G' of the same α is shown in blue dashed lines for comparison (arbitrary offset). Note that outside the range probed by the first 5 PCs the model deviations continue to grow linearly and oscillating features in G'_5 do not necessarily imply features in the underlying G'.

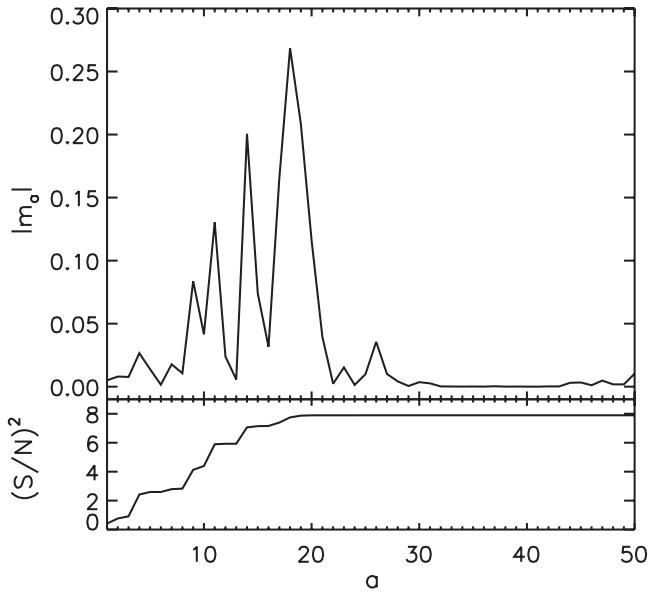

FIG. 12. Principal component amplitudes for the step function potential model [5] that best fit the glitches in the temperature spectrum at $\ell \sim 20$–40 (upper panel), and projected cumulative $(S/N)^2 = \sum (m_a/\sigma_a)^2$ (lower panel). Given the large values of m_a in the high-order PC components, ~20 PCs are required to completely characterize this model.

As an example, the full 50 PC decomposition of the step function potential model from [5] which fits the $\ell = 20$–40 glitches in the temperature power spectrum is shown in Fig. 12. Interestingly, $m_4 = 0.0266$ in the step model and has the highest amplitude of the first 5 components. On the other hand, a complete analysis based on signal-to-noise would require $\sim$20 PC components. By keeping only 5 components, the improvement compared with the ML PL model is only $\Delta\chi^2 = -1.7$. In other words, the step function model is certainly allowed by our 5 PC constraint and even marginally favored but the majority of the improvement is not captured by the truncated analysis.

Nevertheless, when interpreted as an upper limit on deviations from scale-free conditions, the 5 PC approach works as a general, albeit typically conservative, method to constrain a wide variety of possible deviations from a single analysis. As the running of the tilt example shows, the results are remarkably close to a direct analysis and differences can be used to expose the self-consistency of the model inferences with independent parts of the data.

VI. DISCUSSION

We have employed a variant of the generalized slow-roll approximation (GSR) that allows large amplitude deviations from scale-free conditions to place functional constraints on the GSR source function and implicitly on the inflaton potential. By employing a principal component (PC) decomposition, we isolated the 5 best functional constraints imposed by the WMAP7 data. The analysis is greatly facilitated by our optimization of the WMAP7 likelihood code which we have made publicly available [31].

These 5 PCs provide incisive constraints on the inflaton potential around the e-folds of inflation when the scales associated with the first acoustic peak were crossing the horizon. Nonzero values for their amplitudes represent deviations from slow-roll and power law initial spectra. The first component implies that deviations are less than $\sim$3% near $\eta \sim 10^2$ Mpc and the first 5 represent constraints around that scale at better than the 10% level. The result is 5 nearly independent Gaussian constraints that can be applied to any inflationary model where this level of deviation is expected. We have also made the eigenfunctions, which are required to project a given model onto the PC amplitudes, publicly available. These limits are robust to the inclusion of tensor contributions allowed by current B-mode limits, spatial curvature and Sunyaev-Zel'dovich contamination from unresolved clusters.

Interestingly, for the 4th principal component the null prediction of scale-free initial conditions is disfavored at the 95% CL. However, given the 5 added parameters, this result does not rule out a power law initial spectrum at a significant level. Moreover, the relatively large deviations implied by this anomalous mode are allowed only through correspondingly large variations in the cosmological parameters, mainly the cold dark matter and its effect on the sound horizon and by inference the distance to recombination.

Further information from the CMB polarization and high-ℓ temperature power spectrum can break this degeneracy. The QUAD polarization data already have some impact on the constraint and the Planck satellite should definitively resolve this issue. External data also can break this degeneracy. In particular in a flat ΛCDM cosmology, the distance to high redshift supernovae reduce the preference for finite m_4 from 1.9σ to 1.2σ. However this improvement disappears if spatial curvature is marginalized.

This anomalous 4th PC resembles a *local* running of the tilt around scales of $\eta \sim 300$ Mpc. Direct analysis of a *global* constant running of the tilt shows that this preference is mainly local, i.e. the low and high multipoles prefer a different and smaller running than the intermediate multipoles that the first 5 PCs probe. The running of the tilt example illustrates the use of the PC constraints both as a technique to constrain inflationary parameters arising from different models with a general analysis and as a method for examining what aspects of the data drive the constraints.

The running of the tilt example also illustrates that for models where deviations from scale-free conditions become much larger than $\sim$10% away from the well-constrained region of the acoustic peaks, more principal components are required to ensure a complete and incisive description. We intend to examine these issues in a future work.

ACKNOWLEDGMENTS

We thank Michael Mortonson, Eric Switzer and Amol Upadhye for useful conversations. This work was supported by the KICP under NSF Contract No. PHY-0114422. W. H. was additionally supported by DOE Contract No. DE-FG02-90ER-40560 and the Packard Foundation.

APPENDIX A: FAST WMAP LIKELIHOOD EVALUATION

In this Appendix, we describe the optimization of the WMAP likelihood code and fast approximate techniques for describing the low-ℓ polarization information. Changes in the initial power spectrum do not require recomputation of the radiation transfer function and are so-called fast parameters for CosmoMC. Hence the WMAP7 likelihood computation is the main bottleneck for the MCMC analysis.

We first OpenMP parallelize the likelihood code and remove bottlenecks in the computation of the temperature and high-ℓ polarization likelihood. We obtain a $\sim 2.6 N_{\rm core}$ speedup of those parts of the likelihood where $N_{\rm core}$ is the

number of cores in a shared memory machine. These changes exactly preserve the accuracy of the likelihood evaluation.

In place of the computationally expensive low-ℓ polarization pixel likelihood, we seek a fast but accurate approximation. The WMAP team has shown that most of the information in the power law ΛCDM parameter space lies in multipoles $\ell \sim 2$–7 as essentially an overall amplitude of power [27]. However, in the broader parameter space allowed by the PCs of G', we find that a single amplitude is insufficient to describe the information content of the pixel likelihood.

Instead we fit the likelihood function to a two-band approximation

$$p_{Ei} = \left(\frac{1}{\Delta\ell_i}\sum_{\ell=\ell_{i\,\mathrm{min}}}^{\ell_{i\,\mathrm{max}}}\frac{\ell(\ell+1)C_\ell^{EE}}{2\pi}\right)^{1/2}, \tag{A1}$$

where the first band $i = 1$ has $\ell_{1\,\mathrm{min}} = 4$, $\ell_{1\,\mathrm{max}} = 6$ and the second band $i = 2$ has $\ell_{2\,\mathrm{min}} = \ell_{2\,\mathrm{max}} = 8$ and $\Delta\ell_i = \ell_{i\,\mathrm{max}} - \ell_{i\,\mathrm{min}} + 1$ normalizes the parameter to reflect the average bandpower. We find that the pixel likelihood is well approximated by a Gaussian in these two bands for the models under consideration

$$-2\ln\mathcal{L}_{\mathrm{pol}}^{\ell<24} \approx A + (\mathbf{p}_E - \bar{\mathbf{p}}_E)^T\mathbf{C}^{-1}(\mathbf{p}_E - \bar{\mathbf{p}}_E) \tag{A2}$$

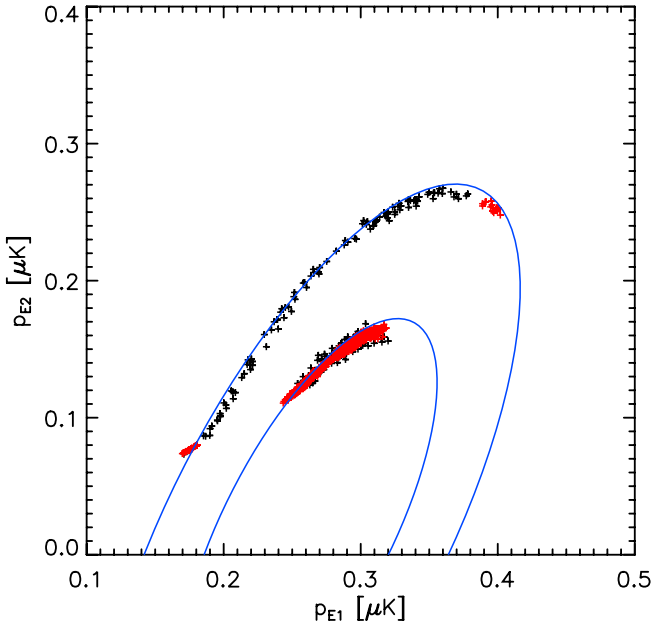

FIG. 13 (color online). Comparison of the low-ℓ polarization pixel likelihood $-2\ln\mathcal{L}_{\mathrm{pol}}^{\ell<24}$ and the approximate fit as a function of E-mode polarization amplitude in two multipole bands p_{E1} ($\ell = 4$–6), p_{E2} ($\ell = 8$). Models from a power law chain (red crosses) and from a 5 PCs chain (black crosses) with likelihood relative to the minimum 1645.84 (within ± 0.1) of 2.29 (68.27% CL) and 6.18 (95.45% CL) are shown with the contours from the fit overplotted (blue curves).

with the parameters $p_{E1} = 0.2614\ \mu$K, $p_{E2} = 0.01955\ \mu$K, $A = 1645.84$

$$\mathbf{C}^{-1} = \begin{pmatrix} 498.31 & -214.23 \\ -214.23 & 190.23 \end{pmatrix} \mu\mathrm{K}^{-2}. \tag{A3}$$

In Fig. 13 we show the accuracy of the fit compared with the pixel likelihood for both power law models and models with additional 5 PCs of G'. Note that the power law models lie on a 1D curve in this space and can be well parametrized by a single amplitude whereas the 5PC models do not. In fact, in the two-band space models with low p_{E1} and high p_{E2} that populate a direction nearly orthogonal to the power law models are more strongly constrained than the total power at low ℓ would suggest. Since this approximation has trivial computational cost, the net improvement in speed is approximately $\sim 5N_{\mathrm{core}}$.

For the cases of interest, the approximation works remarkably well. As an example, we have run an MCMC chain with the exact pixel likelihood for the 5PC chain with WMAP data only. In Fig. 14, we compare the posterior

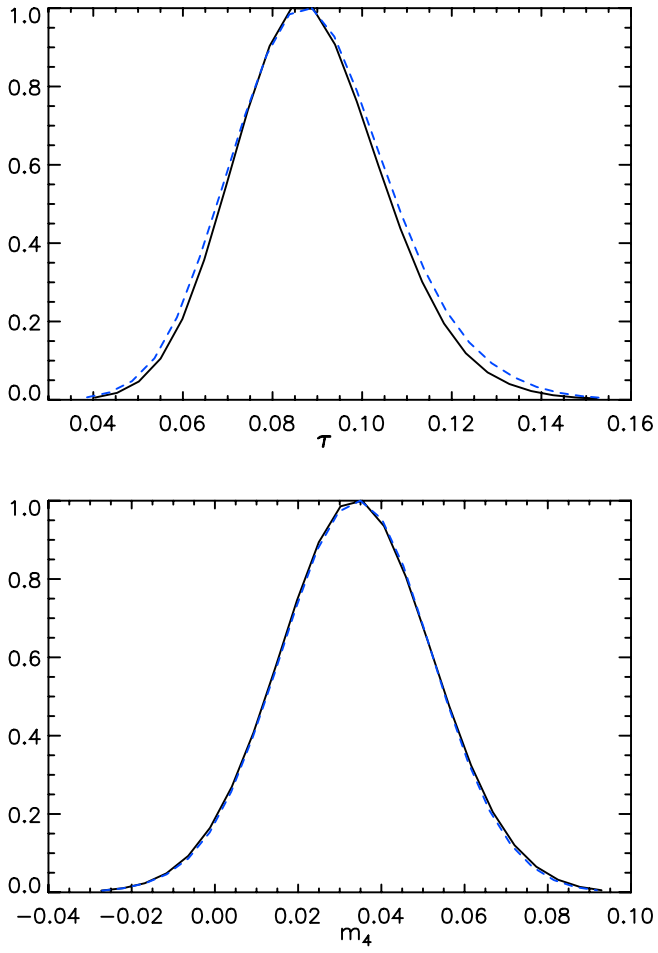

FIG. 14 (color online). Posterior probability distribution of the optical depth τ and the fourth PC amplitude using the exact likelihood (black curves) and the approximation (blue dashed curves) with WMAP data only.

probability distribution of the optical depth τ and m_4 using the full likelihood and the approximation. The difference between the pixel likelihood and the approximation for the 5 PCs maximum likelihood model with WMAP data is likewise negligible: $|2\Delta \ln \mathcal{L}| = 0.05$.

We have also checked that the likelihood approximation remains valid to 10% or better in the $(2\Delta \ln \mathcal{L})^{1/2}$ significance of differences between models with varying reionization history as parametrized by ionization principal components [32].

Larger differences can occur for models with sharp, order unity, initial power spectrum features at the horizon scale. These project onto the temperature and polarization spectra differently and lead to qualitatively different results for the temperature-polarization cross spectrum. In this case one can get discrepancies of order unity in $2\Delta \ln \mathcal{L}$ that err on the side of allowing discrepant models. Even these differences can typically be taken into account via importance sampling at a much smaller computational cost than evaluating the exact pixel likelihood during the MCMC run itself.

[1] C. L. Bennett *et al.* (WMAP), Astrophys. J. Suppl. Ser. **148**, 1 (2003).
[2] H. V. Peiris *et al.* (WMAP) Astrophys. J. Suppl. Ser. **148**, 213 (2003).
[3] L. Covi, J. Hamann, A. Melchiorri, A. Slosar, and I. Sorbera, Phys. Rev. D **74**, 083509 (2006).
[4] J. Hamann, L. Covi, A. Melchiorri, and A. Slosar, Phys. Rev. D **76**, 023503 (2007).
[5] M. J. Mortonson, C. Dvorkin, H. V. Peiris, and W. Hu, Phys. Rev. D **79**, 103519 (2009).
[6] C. Pahud, M. Kamionkowski, and A. R. Liddle, Phys. Rev. D **79**, 083503 (2009).
[7] M. Joy, A. Shafieloo, V. Sahni, and A. A. Starobinsky, J. Cosmol. Astropart. Phys. 06 (2009) 028.
[8] C. Dvorkin and W. Hu, Phys. Rev. D **81**, 023518 (2010).
[9] D. K. Hazra, M. Aich, R. K. Jain, L. Sriramkumar, and T. Souradeep, arXiv:1005.2175.
[10] E. D. Stewart, Phys. Rev. D **65**, 103508 (2002).
[11] J. Choe, J.-O. Gong, and E. D. Stewart, J. Cosmol. Astropart. Phys. 07 (2004) 012.
[12] S. Dodelson and E. Stewart, Phys. Rev. D **65**, 101301 (2002).
[13] W. Hu and T. Okamoto, Phys. Rev. D **69**, 043004 (2004).
[14] S. M. Leach, Mon. Not. R. Astron. Soc. **372**, 646 (2006).
[15] C. Sealfon, L. Verde, and R. Jimenez, Phys. Rev. D **72**, 103520 (2005).
[16] P. Paykari and A. H. Jaffe, Astrophys. J. **711**, 1 (2010).
[17] G. Nicholson, C. R. Contaldi, and P. Paykari, J. Cosmol. Astropart. Phys. 01 (2010) 016.
[18] S. L. Bridle, A. M. Lewis, J. Weller, and G. Efstathiou, Mon. Not. R. Astron. Soc. **342**, L72 (2003).
[19] H. V. Peiris and L. Verde, Phys. Rev. D **81**, 021302 (2010).
[20] K. Kadota, S. Dodelson, W. Hu, and E. D. Stewart, Phys. Rev. D **72**, 023510 (2005).
[21] http://lambda.gsfc.nasa.gov.
[22] N. Christensen, R. Meyer, L. Knox, and B. Luey, Classical Quantum Gravity **18**, 2677 (2001).
[23] A. Kosowsky, M. Milosavljevic, and R. Jimenez, Phys. Rev. D **66**, 063007 (2002).
[24] A. Gelman and D. Rubin, Stat. Sci. **7**, 452 (1992).
[25] A. Lewis and S. Bridle, Phys. Rev. D **66**, 103511 (2002).
[26] http://cosmologist.info/cosmomc.
[27] D. Larson *et al.*, arXiv:1001.4635.
[28] H. C. Chiang *et al.*, Astrophys. J. **711**, 1123 (2010).
[29] http://www.supernova.lbl.gov/Union.
[30] A. G. Riess *et al.*, Astrophys. J. **699**, 539 (2009).
[31] http://background.uchicago.edu/wmap_fast.
[32] M. J. Mortonson and W. Hu, Astrophys. J. **672**, 737 (2008); see also http://background.uchicago.edu/camb_rpc.